Efficacy of a ZrB$_2$–SiC matrix in protecting C fibres from oxidation in novel UHTCMC materials

L. Zoli, D. Sciti

Highlights

- High density UHTCMCs with 40 ÷ 65% Cf content were produced by slurry infiltration and hot pressing.

- The protective matrix consisted in ultra-refractory ZrB$_2$–SiC ceramic mixtures

- Materials with fully dense matrix had a higher flexural strength (240 MPa) and better oxidation resistance at 1650 °C.

- Materials with weak matrix/fibre interface showed higher toughness (> 10 MPa m$^{0.5}$) but worse oxidation resistance.

Abstract

A series of high density ceramic composites with carbon fibre content between 40 and 65% and ultra-refractory ceramic matrix was produced by slurry infiltration and hot pressing. The matrix consisted of ZrB_2–10 vol% SiC or ZrB_2–40 vol% SiC ceramic mixtures. Water–based and polymer–based routes were tested to analyse the effects on microstructure, mechanical properties and oxidation resistance at 1650 °C in air. Changing the process and/or the processing parameters was found to affect the final composition, the amount of residual porosity, the matrix/fibre adhesion. Composites with nearly fully dense matrix and optimized infiltration of fibre preforms were found to possess the highest strength (240 MPa) and oxidation resistance. Composites with weak interface and higher porosity in the matrix showed higher toughness (up to 12 MPa m$^{0.5}$) but were more prone to oxidation and erosion.

Graphical abstract
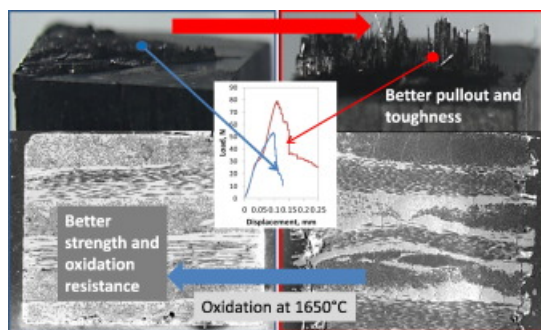
Download high-res image (411KB)   Download full-size image

< **Previous** article   **Next** article >

Keywords

Carbon; ZrB_2; Microstructure; Mechanical properties; Oxidation resistance

1. Introduction

C/C and C/SiC are the materials currently used for aero-engine parts, hot gas valve parts, thermal structures and thermal protection systems (TPSs) [1]. Carbon is one of the materials with the highest temperature resistance and can be used in technical applications up to 2800 °C if kept in non-oxidising environment [1]. SiC is able to offer protection against oxidation at least up to 1600 °C in an oxygen-rich atmosphere, thanks to the development of a SiO_2 surface film, however at temperature > 1600 °C and in low-oxygen atmosphere it develops a substantial vapour pressure. As a matter of fact, the combination of extreme temperature and chemically aggressive environment is beyond the capabilities of current engineering materials.

In recent years, several researchers have proposed the use of ultra-refractory ceramics (UHTCs) such as ZrB_2, HfB_2, ZrC, HfC and TaC as alternative matrix or coating phases to protect C preforms from oxidation and erosion. One common approach adopted is to enrich the composite matrix with UHTC phases (usually with addition of SiC particles) using the combination of different techniques such as: slurry infiltration and CVI [2,3], PIP [4,5,6], PIP and CVI [7,8,9], reactive melt infiltration [10,11]. Some of those authors studied the ablation behaviour of C/C-UHTC composites and reported a notable increase of the erosion resistance compared to conventional C/C materials. [2,3] The efficacy of a UHTC phase in protecting carbon fibres was also demonstrated in our previous studies on the ablation behaviour of ZrB_2–based composite containing 45% of random chopped C fibres [12]. An alternative approach is a surficial infiltration of C/C composites with ZrB_2-SiC mixture to obtain oxidation resistant coatings that were shown to resist to oxidation up to 1600 °C in air [13].

Overall, there is an increasing interest in improving the capability of current engineering materials to withstand harsh environmental conditions introducing the use of ultra-refractory ceramic phases in conventional CMC technologies.

In this paper we produced new composites, the so called UHTCMCs (Ultra-High Temperature Ceramic Matrix Composites) through infiltration of C fibre preforms by ZrB_2-SiC slurries and consolidation by hot pressing method [14]. This approach has been already successfully utilized for processing UHTCMCs with SiC fibres [15,16] or for processing C/SiC composites and has the advantage of being particularly fast (typical two processing days) if compared with conventional CVI–based processes [17]. Two aspects are the focus of the present work:

– on one hand the capability of the ZrB_2-based matrix to impart self-healing properties to the composite, protecting the fibres from excessive degradation in oxidation environment at temperature > 1600 °C;

– on the other the ability of carbon fibres to impart flaw tolerance to brittle ZrB_2-based ceramics.

Two processing routes are investigated:

– a water–based route, where the matrix powders, ZrB_2 and SiC, are dispersed in water;

– a polymer–based route, where ZrB_2 powder is dispersed in a liquid SiC precursor (allyl-hydride-polycarbosilane).

The fibre content ranged from 40 to 65%. Flexural strength and fracture toughness were measured and discussed in relation with fibre amount and fibre/matrix interface. The oxidation resistance was studied through thermal treatment at 1650 °C, in air, for 1 min in a bottom loading air furnace. The efficacy of the matrix to protect the fibre was investigated in terms of fibre/matrix interface, amount of UHTC phase, and robustness of the interface.

2. Experimental

Commercial products were used for the materials preparation: - ZrB_2 (Grade B, H.C. Starck, Germany), specific surface area 1.0 m^2/g, particle size range 0.5–6 µm, impurities (wt.%): 0.25 C, 2.00 O, 0.25 N, 0.10 Fe, 0.20 Hf; - Alpha SiC (Grade UF-25, H.C. Starck, Germany) specific surface area 23–26 m^2/g, D_{50} 0.45 µm; allyl-hydride-polycarbosilane (SMP-10, Starfire System Inc. U.S.A.), density 0.998 g/cm^3, as SiC precursor; commercial high modulus pitch-derived carbon fibre (C_f) preforms were used. The following compositions were prepared according to two different routes.

Water-based route:

1) 35% (90% ZrB_2 + 10% SiC) + 65% C_f, labelled as Z10S-65F;

2) 45% (90% ZrB_2 + 10% SiC) + 55% C_f, labelled as Z10S-55F;

3)   60% (90% ZrB_2 + 10% SiC) + 40% C_f, labelled as Z10S-40F;

Polymer-based route:

4)   45% (60% ZrB_2 + 40% SiC) + 55% C_f, labelled as Z40S-55F.

For the water-based route, a ZrB_2–10 vol% SiC powder mixture was preliminary prepared by wet ball milling in ethanol and subsequent drying. With this mixture, aqueous slurries were prepared according to previous studies [18] using polyacrylates at different molecular weight as dispersants to tailor the fibre volumetric amount. Neither details about the dispersants nor characteristics of the slurries in terms of viscosity are intentionally indicated in this work. The composites were fabricated infiltrating the 1-D fabrics with the slurries by hand lay-up and subsequently stacking 8 layers in a 0–90° configuration. Vacuum-bagging was used to remove air bubbles entrapped in the green composite and to line up the fibres. Hot pressing cycles were then carried out in the range 1800–1900 °C, using a pressure of 30–40 MPa, on the basis of previous studies [14].

For the polymer-based route, a composite was prepared by directly dispersing the ZrB_2 particles into a liquid allyl-hydride-polycarbosilane. Similarly to the previous process, 8 unidirectional fabrics were infiltrated with the slurries by hand lay-up and stacked in a 0–90° configuration. The curing of the polycarbosilane was performed in vacuum bagging at 150 °C for 1 h, after that the pellet was thermally treated (pyrolysis) under argon flux at 800 °C for 30 min in graphite furnace and then hot pressed at the same conditions reported above.

The microstructures were analysed on polished and fractured surfaces by field emission scanning electron microscopy (FE-SEM, Carl Zeiss Sigma NTS Gmbh Öberkochen, Germany) and energy dispersive X-ray spectroscopy (EDS, INCA Energy 300, Oxford instruments, UK). X-ray diffraction Bruker D8 Advance apparatus (Bruker, Karlsruhe, Germany).

After sintering, the bulk density was determined by the Archimede method. The relative density, ρ was thus calculated as the ratio of experimental to theoretical value, and the residual porosity deduced as 1-ρ.

Image analysis (Image-Pro Analyser 7.0) was carried out onto SEM micrographs of polished sintered sections to determine the amounts of SiC, C_f and porosity (see values in Table 1).

Table 1. Compositions, sintering cycles, fibre amount, densities and mechanical properties of the composites.

Label	Process	Composition (vol%)		Density (g/cm³)	Porosity (%)	Flexural strength (MPa)	Fracture toughness (MPa m⁰·⁵)
		ZrB_2-SiC Matrix	C_f				
Z10S-65F	Water-based	90–10	65	2.9	15	140 ± 30	7.5 ± 1.4
Z10S-55F	Water-based	90–10	55	3.3	12	125 ± 35	7.3 ± 0.9
Z10S-40F	Water-based	90–10	40	3.9	8	235 ± 40	6.4 ± 0.8
Z40S-55F	Polymer-based	60–40	55	3.3	4	152 ± 12	10.6 ± 1.6

As for the mechanical properties, 4-pt bending strength tests were carried out for selected compositions according to EN 843-1 (2004) norm for advanced technical ceramics. The test bars, 25 × 2.5 × 2 mm^3 (length by width by thickness, respectively) were fractured using a semi-articulated silicon carbide four-point fixture with a lower span of 20 mm and an upper span of 10 mm using a screw-driven load frame (Instron mod. 6025, Instron, High Wycombe, GB). For each material at least four bars were tested. The fracture toughness (K_{Ic}) was evaluated by fracturing chevron notched beams (CNB), following the guidelines of EN 14425-3 (2010) for advanced technical ceramics. The test bars, 25 mm × 2 mm × 2.5 mm^3 (length by width by thickness, respectively), were notched with a 0.1 mm-thick diamond saw; the chevron-notch tip depth and average side length were about 0.12 and 0.80 of the bar thickness, respectively. The specimens were fractured using a fully-articulated steel four-point fixture with a lower span of 20 mm and an upper span of 10 mm using a screw-driven load frame (Instron, 6025). Three specimens were loaded with a crosshead speed of 0.05 mm/min. The "slice model" equation of Munz et al. [19] was used to calculate K_{Ic}. A bottom loading furnace was used to test the resistance to oxidation of the composites. This furnace allows introducing the samples when the test temperature is reached. This is particularly useful to avoid oxidation of the samples during the heating step. Once introduced in the furnace chamber, 30 s are necessary to reach the thermal equilibrium, then the short isothermal stage begins (1 min). After the end of the oxidation stage, the samples were removed and naturally air quenched.

3. Results and discussion

3.1. Microstructural features

Compositions, sintering cycles, fibre amount and densities of the composites are reported in Table 1. Polished sections of the composites are shown in Fig. 1.
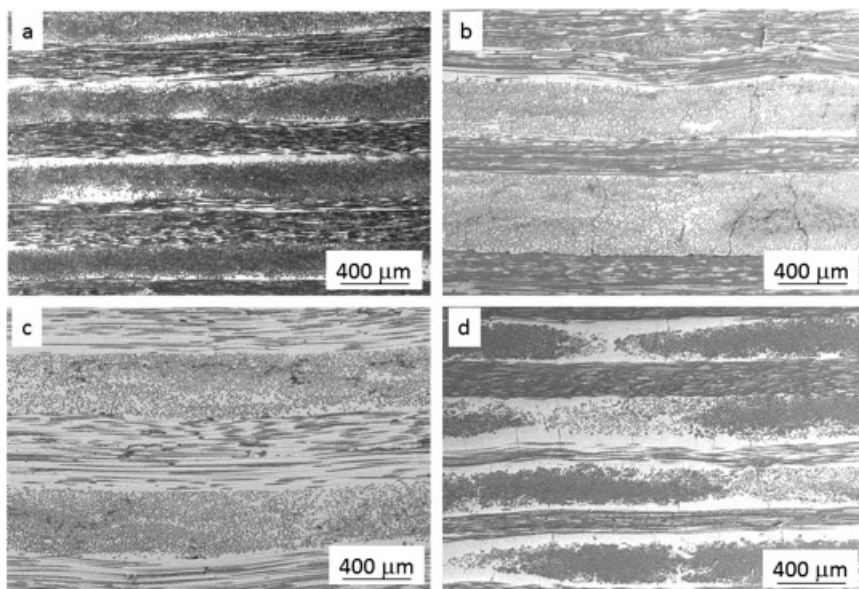
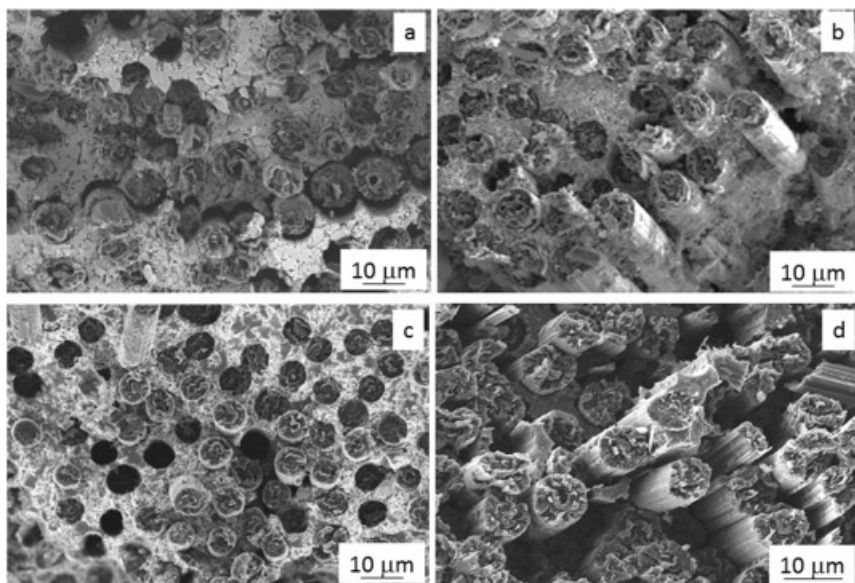Download high-res image (481KB)   Download full-size image

Fig. 1. Polished section of samples: a) Z10S-65F; b) Z10S-55F; c) Z10S-40F, obtained through the water-based route; d) Z40S-55F, obtained through the polymeric-route.

Sample Z10S-65F, with (ZrB$_2$–10% SiC) as matrix and 65% of Cf has a bulk density of 2.9 g/cm^3 and a porosity around 15%. The laminate structure in Fig. 1a, shows that the layers have approximate thickness of 200 μm. The infiltration is not complete, especially in the central area of the bundle. The incomplete densification of the matrix as well as intra bundle voids contribute to the total amount of porosity. Typical defects of these composites are: non-infiltrated areas and cracks in matrix-rich regions. Cracks originate for constrained shrinkage of the matrix during sintering and thermal expansion coefficient mismatch between matrix and fibres (6.5 10^{-6} °C^{-1}[20], 2 10^{-6} °C^{-1}[1], respectively). As for the matrix/fibre interface, a good adhesion was found but no reaction occurred, at least according to the SEM resolution (Fig. 2a). Fracture surfaces (Fig. 3a) show both bundle pull-out and individual pull-out. These features suggest a fibre–matrix debonding mechanism. The extent of fibre pull-out is strictly related to the cohesion between matrix and fibres that developed during the densification process.
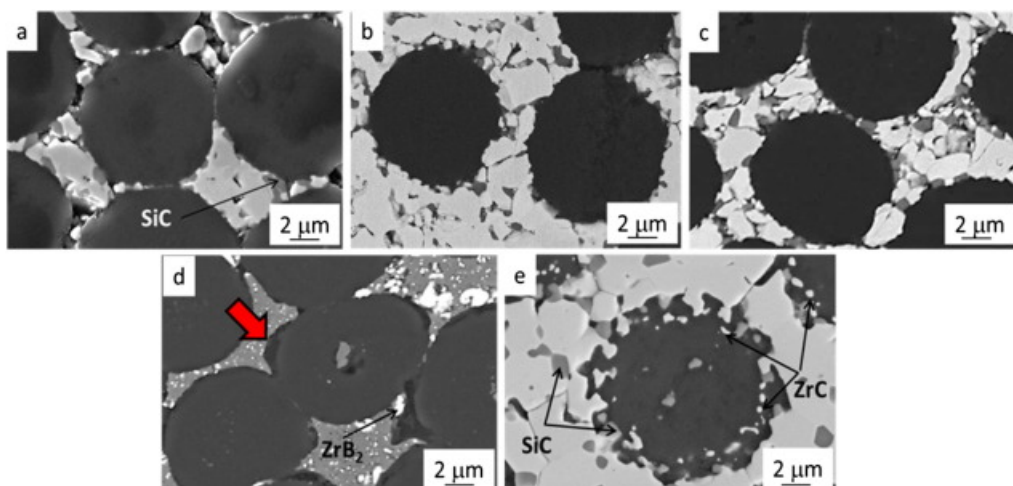
Download high-res image (223KB) Download full-size image

Fig. 2. Details of the matrix-fibre interface for samples: a) Z10S-65F; b) Z10S-55F, c) Z10S-40F, obtained through water-based route, d) Z40S-55F at the C/SiC interface and e) the same sample at the C/ZrB$_2$ interface. The arrow in d) indicates the detachment of the SiC phase from the carbon fibre.

Download high-res image (406KB)   Download full-size image

Fig. 3. Fracture surfaces showing pull-out for samples: a) Z10S-65F; b) Z10S-55F; c) Z10S-40F, obtained through the water-based route; d) Z40S-55F, obtained through the polymeric-route.

Sample Z10S-55F: This composite with a (ZrB$_2$-10% SiC) matrix and 55% C$_f$ has a bulk density of 3.3 g/cm^3 and a residual porosity of 12%, Table 1. Tailoring the slurry viscosity allowed a very good degree of infiltration inside the fibre bundles by the matrix. Due to enhanced penetration of the slurry, the thickness of each individual layer is higher than the previous case, 300–400 μm, Fig. 1b. Typical defects of this composite are transverse cracks due to tensile stress in the matrix and delamination (not shown). As for the previous case, the extent of matrix – fibre reaction is very limited (Fig. 2b) and this facilitates the fibre pull-out during fracture (Fig. 3b).

Sample Z10S-40F: This composite with a (ZrB$_2$-10% SiC) matrix and 40% C$_f$ has the highest density, 3.9 g/cm^3, and the lowest residual porosity, about 8%. The typical layer thickness is > 400 μm, Fig. 1c. The higher bulk density is due to a lower content of fibres and a better matrix densification, Fig. 2c. Due to high homogeneity of the infiltration, the amount of cracks and delamination is reduced compared to the previous samples. On the other hand, the better degree of densification even in the intra-bundle region, seems to reduce the extent of fibre pull-out compared to the other samples (see an example in Fig. 3c) probably due to enhanced adhesion of the fibre to the matrix.

Sample Z40S-55F: The composite obtained through the polymeric route, with a (ZrB$_2$-40% SiC) matrix and 55% C$_f$ has a bulk density of 3.3 g/cm^3 and residual porosity lower than 5%, Table 1. In the overview of Fig. 1d, it is apparent that the texture is less homogeneous compared to the previous materials. The tows are generally completely infiltrated, but in the central regions they are prevalently infiltrated by the polycarbosilane, whilst towards the external part of the bundles, ZrB$_2$ is the major constituent phase. Two different interfaces were thus created for this composite: one intra-bundle C$_f$/SiC interface and an inter-bundle C$_f$/ZrB$_2$ interface, see Fig. 2d,e. The C$_f$/SiC interface is relatively smooth (Fig. 2d), and partial detachment of the SiC phase from the C$_f$ is often observed (see arrow in Fig. 2d). According to previous works on C$_f$/SiCN minicomposites [21] we hypothesize that these defects are due to the shrinkage occurring during pyrolysis of polycarbosilane. On the contrary, for carbon fibres embedded into the ZrB$_2$ matrix, the fibre profile became jagged and a sort of interlocking between ZrB$_2$ grains and C$_f$ was observed (Fig. 2e). Furthermore, ZrC and SiC grains were embedded

in the fibres. This jagged profile was attributed to the cooperation of different phenomena. Due to the different CTE of ZrB_2, SiC and Cf a complex pattern of compressive and tensile stresses developed in this composite. C/SiC areas were under compression, whist ZrB_2-rich regions under tension. Thus, isolated fibres into ZrB_2 regions underwent a radial compression by the ZrB_2 phases, which resulted in the observed morphology. At the same time, liquid phase based on Si-O-Zr penetrated in the outer layers of the carbon fibres and reacted with carbon forming ZrC and SiC particles, as observed in [22]. As a consequence of this complex morphology, the fibre pull-out was more pronounced at the C_f/SiC interface (see Fig. 3d) than at the fibre/ZrB_2 interface (not shown).

3.2. Mechanical behaviour

As previously mentioned, sample bars for mechanical testing were machined from the sintered pellets by diamond tool machining. Furthermore, since these composites have a sintered matrix, we opted for the characterization methods typical of advanced ceramics, instead of CMCs. The flexural strength of the four UHTC-composites ranges from 120 to 240 MPa. The values obtained are in agreement with those found in the literature: H. Hu in [4] reported a flexural strength of 163 MPa for a C/SiC material enriched with about 25% of ZrB_2, Q. Li [5] reported a bending stress of 248 MPa for a 3D-C/SiC enriched with 23% of ZrB_2-ZrC phases, L. Li [8] found a value of 255 MPa for 2D-C/SiC enriched with a ZrB_2-TaC mixture.

The flexural strength does not increase with increasing the amount of fibre, in contrast with findings in the literature [17]. Indeed, samples Z10S-65F, Z10S-55F, Z40S-55F, with higher fibre content, 65 and 55%, have lower strength (120–150 MPa) than composite Z10S-40F containing just 40% of fibres, 240 MPa. Flexural strength of these composites seems to be affected by other factors:

–   the localized damage due the machining of the bars, that introduced surface defects and scratches in the fibres; furthermore due to the non-perfect alignment of laminate planes, the machined bar surface can be a patchwork of areas with fibres parallel and perpendicular to the loading direction;

–   the content of fibres in the axial/transverse direction can vary between different bars;

–   the presence of shear stresses due to non-optimized ratio between span and bar thickness.

As a result, a large data dispersion is observed especially for composites Z10S-65F, Z10S-55F (21 and 28%, respectively).

The fracture toughness measured through CNB in flexure, ranged from 6.4 ± 0.8 MPa m$^{0.5}$ of the most dense sample (Z10S-40F) to 10.6 ± 1.6 MPa m$^{0.5}$ for sample Z40S-55F, in agreement with data reported in the literature on C/SiC/ZrB_2[4] and C/ZrC composites [10]. A comparison of typical load/displacement curves recorded for the four samples is shown in Fig. 4a, whilst the extent of fibre pull-out is reported in the optical pictures of Fig. 4b–e. Again the toughness can be affected by several factors: for instance, the higher values found for samples Z10S-65F and Z10S-55F compared to Z10S-40F could be due to the higher amount of fibres for the former (65 and 55%, respectively) and the stronger interface of the latter (compare for instance the lower extent of fibre pull-out of this sample in Fig. 4d, with respect to sample Z10S-65F in Fig. 4b). The higher amount of fibres induces more residual stress in the matrix with consequent cracking and decrease of the matrix modulus, which applies for Z10S-65F and Z10S-55F. The decrease of the matrix modulus is also induced by the higher amount of porosity, which occurs for sample Z10S-65F; both these two factors positively affect the value of fracture toughness. Sample Z40S-55F has a markedly higher value of toughness, which is likely related to the characteristics of the fibre/matrix interface, in particular to the ability of the C/SiC interface to promote more fibre pull-out than a ZrB_2/C interface, see Fig. 4e. An interesting feature of this sample is the correlation between the data of fracture toughness and the notch tip positioning, as observed in the post test optical analysis. Higher values of fracture toughness (> 10 MPa m$^{0.5}$) were found when the tip was located inside the SiC/C_f areas under compressive stresses and lower (< 10 MPa m$^{0.5}$) when the tip was positioned in ZrB_2-rich areas, under tensile stresses.
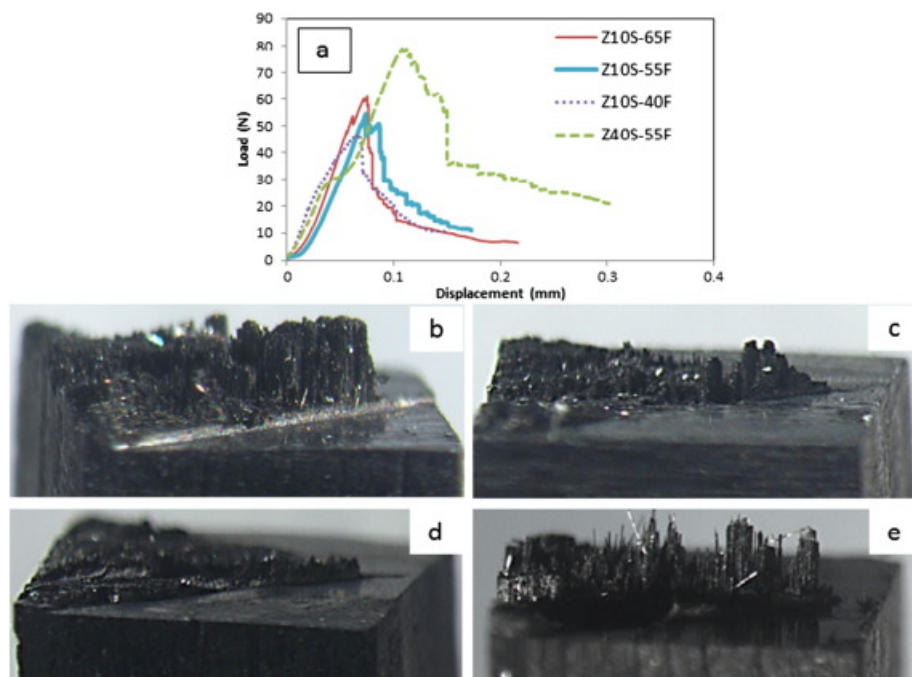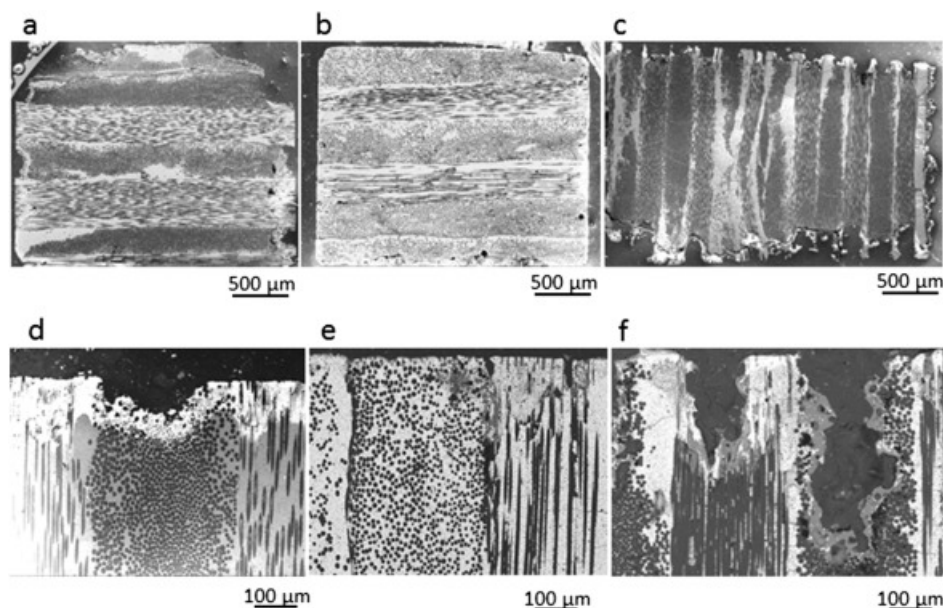
Download high-res image (252KB)   Download full-size image

Fig. 4. a) Comparison of load/displacement curves, b–e) the fracture surface of the notch after CNB tests for samples, b) Z10S-65F; c) Z10S-55F; d) Z10S-40F; e) Z40S-55F.

3.3. Oxidation behaviour

All the samples were exposed to air at 1650 °C, for 1 min. Fig. 5 compares polished cross sections of samples Z10S-55F, Z10S-40F, Z40S-55F. The main phenomena occurring during exposition were oxidation of the matrix phases, e.g. ZrB_2 and SiC, and of the fibres according to:

$$ZrB_2 + 5/2O_2\,(g) = ZrO_2 + B_2O_3\,(l) \tag{1}$$

$$SiC + 3/2O_2\,(g) = SiO_2\,(l) + CO\,(g) \tag{2}$$

$$C + 1/2O_2\,(g) = CO\,(g) \tag{3}$$

Fig. 5. Oxidized cross sections (1 min at 1650 °C) of samples, (a, d) Z10S-55F, (b, e) Z10-40F, (c, f) Z40S-55F.

ZrB_2 starts to oxidize at 600 °C with formation of solid ZrO_2 and liquid B_2O_3 whilst carbon fibres start to vaporize significantly a T > 700 °C. The addition of SiC improves the oxidation resistance at temperatures above 1200 °C by promoting the formation of a borosilicate layer, which reduces the oxygen permeability on exposed surfaces. The oxidation resistance was very different amongst the composites, being affected by a residual porosity, amount of C fibres and amount of SiC phase.

Sample Z10S-65F with 65% of C fibres and 3.5 % of SiC phase (overall) was severely attacked by oxidation (not shown), due to the presence of a high amount of residual porosity and non-infiltrated intra-tow areas. Analysis of the surface confirmed that the oxygen penetrated in the voids of intra-bundle regions, causing fast vaporization of fibres and leaving a layer of porous ZrO_2. The sample cross section was difficult to prepare due to excessive brittleness.

Sample Z10S-55F, with nominally 55% of fibres and 4.5% of SiC phase (overall) showed a better resistance compared to previous sample, even if the oxidation and erosion affected the sample up to about 250 μm in depth. SiC addition helped forming a somewhat discontinuous surface silica layer. Defective areas such as cracks, as well as intra-tow voids led to enhanced penetration of oxygen. On the section (Fig. 5a,d) the scale profile was quite irregular, with more or less damaged/oxidized zones depending on local arrangements of fibre/matrix, presence of cracks or voids.

For **Sample Z10S-40F** containing 40% of carbon fibres and 6% of SiC phase (overall), an almost continuous outer layer of silica was observed on the surface (Fig. 5b,e). Exposure of these samples to air resulted in a layered morphology similar to what observed for ZrB_2-SiC composites containing graphite [23]. After exposition of 1 min, the sample was topped by a non-continuous layer of SiO_2. Underneath this layer a ZrO_2-SiO_2 scale was found, where silica often replaced voids left by fibre evaporation. Below, C_f

were immersed in a ZrO_2 scale until the unaffected bulk was reached. For this sample, the outer layer of ZrO_2 and silica could offer a significant protection to the carbon fibres. Moreover, voids left by evaporation of fibre located on/near the surface were partially filled with borosilicate phase diffusing towards the surface.

Sample Z40S-55F with 55% of carbon fibres and about 18% of SiC phase (overall) underwent a strong erosion, which was more marked in fibre-rich regions infiltrated with the SiC precursor (Fig. 5c,f). Carbon fibres embedded in SiC-rich regions were more eroded than those embedded in ZrB_2 –rich regions. This could be due to the different composition of the oxide scale formed: in ZrB_2-rich regions, a ZrO_2-rich layer with a borosilicate glass filling the holes was observed. On the contrary, when SiC-rich areas were exposed to air the formation of SiO_2 was less efficient in protecting the C fibres from fast evaporation.

4. Discussion: factors affecting the capability of the UHTC matrix to protect the fibres

A strongly recommended functionality for materials to be used in extreme environments is self-healing capability and self-protection. For bulk ceramics, self-healing is intended to be the partial or complete sealing of cracks through a thermal treatment (also called crack-healing). Much more recently, a self-healing ability has been invoked for UHTCs ceramics when 10–20 vol% SiC-based phases are added to UHTC matrices (e.g. ZrB_2 and HfB_2). Self-protection is triggered by surface-oxidation which results in the formation of a compact protective borosilicate layer [24]. In the bulk, oxidation products can easily penetrate into defects and flaws, thus leading to cracks being blunted and healed.

For UHTCMCs to be operated in harsh aerospace environment, the self-healing/self-protection capability is reached with the in-situ external formation of an adherent ultra-refractory solid oxide scale, essentially the oxidation product of the UHTC matrix, and simultaneous filling of voids by a liquid oxidation product in the bulk.

Within the samples developed in the present work, only the composite with 40% of fibres, namely Z10S-40F, seems to display this capability. This is due to multiple factors:
I)   due to optimized infiltration, all C fibres are circumvented by the protective ZrB_2 matrix;

II)   the matrix has very low porosity (< 10%);

III)   an homogenous distribution of SiC phase is achieved in the ZrB_2 matrix;

IV)   a good cohesion is found at the ZrB_2/C_f interface.

Factor I suggests that volumetric amount of protective UHTC phase must be appropriately calibrated: the requirement is that each individual fibre is surrounded by a shell of protective matrix grains. This, in turn, affects the minimum fibre/fibre distance which is correlated with the mean particle diameter and mean fibre diameter, respectively. With a simple geometric calculation it was estimated that with a ZrB_2 grain size of ~ 2.5 µm and fibre diameter of ~ 10 µm, the minimum matrix amount to allow fibre coating with at least one layer of (ZrB_2-SiC) particles is about 50%. Indeed, only Z10S-40F satisfies this criterion, whilst for samples Z10S-65F and Z10S-55F the amount of fibres (65 and 55%) is too high to have a uniform coating by the matrix (35 and 45% respectively), resulting in poor resistance to oxidation. The overall amount of SiC in the composite is also important to impart self-healing properties. In samples Z10S-55F and Z10S-40F, the presence of 4.5% and 6% SiC, respectively, favour the formation of borosilicate glass that diffuse across the scale, closing ZrO_2 scale porosity as well as voids left by cracks or fibre evaporation. For lower content of SiC (as in Z10S-65F, where the total amount of SiC is ~ 3.5%), the oxide is too friable and tends to detach from the bulk.

A particular case is that of sample Z40S-55F in which the addition of SiC is obtained through a polycarbosilane. As previously shown, the fibre tow is preferably infiltrated by the SiC-rich phase containing a small amount of fine grained ZrB_2 particles, whilst larger ZrB_2 particles remain in inter-tow regions. In this case, oxidation tests confirmed that a ZrB_2-rich matrix is more efficient in protecting the carbon fibre than a SiC-rich matrix, thus intra-tow regions where the fibres are mainly coated by the SiC phase are strongly

eroded. The protective action of the ceramic phase is also jeopardized by the partial detachment of SiC from C fibres, occurring during pyrolysis. Voids are indeed preferred paths for the oxygen diffusion.

It is interesting to compare the performance of the four samples analysed. To this aim, the plot of Fig. 6 shows the relative amounts of ZrB_2, SiC, Cf and porosity (normalized values).
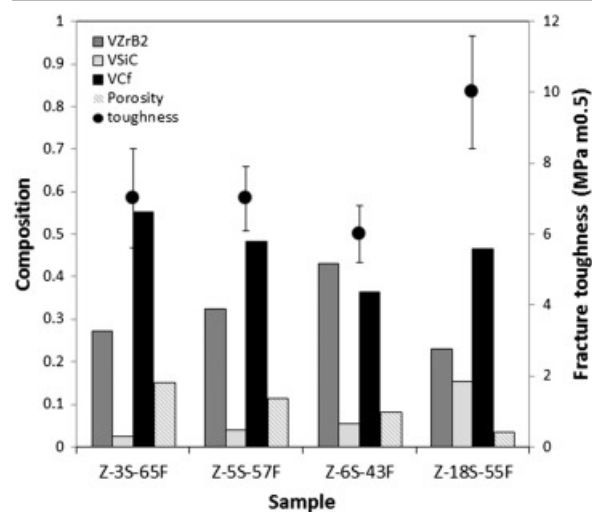
Fig. 6. The plot shows the toughness and the relative amounts of ZrB_2, SiC, C_f and porosity (normalized values) of the four samples.

It can be clearly seen that going from sample Z10S-65F to Z10S-40F there is an increase of ZrB_2 and decrease of C fibres and porosity. On one hand, sample Z10S-40F has the best oxidation resistance - due to low porosity, low cracking, calibrated amount of fibres - and the lowest fracture toughness - due to stronger interface and high matrix modulus. On the other hand, the partially porous ZrB_2-matrices in samples Z10S-65F and Z10S-55F favour high values of fracture toughness due to both decrease of matrix Young's modulus and weak fibre/matrix interface, but presence of porosity jeopardizes the resistance to oxidation/erosion. The addition of the SiC-precursor generates an intra-bundle SiC/C interface, which increases the mechanical properties (fracture toughness) but a SiC-rich matrix offers a worse protection for C fibres with respect to the ZrB_2- rich matrix.

With the research conducted so far, a higher fracture toughness is achieved at the expenses of the oxidation resistance. If oxidation/erosion resistance is the primary requirement, suitable fibre content vs UHTC phase content, dense matrices and a good adhesion between fibre and matrix seem to be preferable.

5. Conclusions

In this paper, we critically analysed the performance of novel UHTCMCs with variable C_f content (40–65%) and SiC phase content (3.5–18%), focusing on the capability of the ZrB_2-based matrix to protect the fibres from oxidation at 1650 °C. We demonstrated that for an efficient protection the carbon fibres should be uniformly coated by the protective

UHTC-SiC matrix.

The research conducted also revealed that there is a trade-off between oxidation resistance and fracture toughness. A dense UHTC matrix is accompanied by a relatively strong ZrB_2-C_f interface offering a good oxidation protection but implying a lower value of fracture toughness. On the other hand, a partially porous ZrB_2-matrix leads to high values of fracture toughness due to both decrease of matrix Young's modulus and weak fibre/matrix interface, but presence of porosity jeopardizes the resistance to oxidation/erosion. The addition of SiC through a liquid precursor generates an intra-bundle SiC/C interface, which increases the mechanical properties (fracture toughness) but a SiC-rich matrix offers a worse protection for C fibres with respect to the ZrB_2-rich matrix.

Acknowledgements

Recommended articles   Citing articles (11)

References

[1]   W. Krenkel (Ed.), Ceramic Matrix Composites: Fibre Reinforced Ceramics and Their Application, Wiley-Vch.Verlag GmbH&Co, Weinheim (2008)
(ISBN: 978-3-527-31361-7)

[2]   A. Paul, S. Venugopal, J.G.P. Binner, B. Vaidhyanathan, A.C.J. Heaton, P.M. Brown
UHTC–carbon fibre composites: preparation, oxyacetylene torch testing and characterization
J. Eur. Ceram. Soc., 33 (2013), pp. 423-432, 10.1016/j.jeurceramsoc.2012.08.018
Article   Download PDF   View Record in Scopus   Google Scholar

[3]   S. Tang, J. Deng, S. Wang, W. Liu, K. Yang
Ablation behaviors of ultra-high temperature ceramic composites
Mater. Sci. Eng. A, 465 (2007), pp. 1-7, 10.1016/j.msea.2007.02.040
Article   Download PDF   CrossRef   View Record in Scopus   Google Scholar

[4]   H. Hu, Q. Wang, Z. Chen, C. Zhang, Y. Zhang, J. Wang
Preparation and characterization of C/SiC-ZrB_2 composites by precursor infiltration and pyrolysis process
Ceram. Int., 36 (2010), pp. 1011-1016, 10.1016/j.ceramint.2009.11.015
Article   Download PDF   View Record in Scopus   Google Scholar

[5]   Q. Li, S. Dong, Z. Wang, G. Shi
Fabrication and properties of 3-D C_f/ZrB_2-ZrC-SiC composites via polymer infiltration and pyrolysis
Ceram. Int., 39 (2013), pp. 5937-5941, 10.1016/j.ceramint.2012.11.074
Article   Download PDF   View Record in Scopus   Google Scholar

[6]   D. Zhao, C. Zhang, H. Hu, Y. Zhang

Preparation and characterization of three-dimensional carbon fibre reinforced zirconium carbide composite by precursor infiltration and pyrolysis process

Ceram. Int., 37 (2012), pp. 2089-2093, 10.1016/j.ceramint.2011.02.024

Google Scholar

[7]   Y. Wang, W. Liu, L. Cheng, L. Zhang

Preparation and properties of 2D C/ZrB$_2$–SiC ultra high temperature ceramic composites

Mater. Sci. Eng. A, 524 (2009), pp. 129-133, 10.1016/j.msea.2009.07.005

Article   Download PDF   CrossRef   View Record in Scopus   Google Scholar

[8]   L. Li, Y. Wang, L. Cheng, L. Zhang

Preparation and properties of 2D C/SiC–ZrB$_2$–TaC

Ceram. Int., 37 (2011), pp. 891-896, 10.1016/j.ceramint.2010.10.033

Article   Download PDF   View Record in Scopus   Google Scholar

[9]   Z. Wang, S. Dong, X. Zhang, H. Zhou, D. Wu, Q. Zhou, D. Jiang

Fabrication and properties of Cf/SiC-ZrC composites

J. Am. Ceram. Soc., 91 (2008), pp. 3434-3436, 10.1111/j.1551-2916.2008.02632.x

CrossRef   View Record in Scopus   Google Scholar

[10]   S. Chen, C. Zhang, Y. Zhang, H. Hu

Influence of pyrocarbon amount in C/C preform on the microstructure and properties of C/ZrC composites prepared via reactive melt infiltration

Mater. Des., 58 (2014), pp. 570-576, 10.1016/j.matdes.2013.12.071

Article   Download PDF   View Record in Scopus   Google Scholar

[11]   M. Kütemeyer, L. Schomer, T. Helmreich, S. Rosiwal, D. Koch

Fabrication of ultra high temperature ceramic matrix composites using a reactive melt infiltration process

J. Eur. Ceram. Soc., 36 (2016), pp. 3647-3655, 10.1016/j.jeurceramsoc.2016.04.039

Article   Download PDF   View Record in Scopus   Google Scholar

[12]   D. Sciti, L. Zoli, L. Silvestroni, A. Cecere, G.D. Di Martino, R. Savino

Design, fabrication and high velocity oxy-fuel torch tests of a Cf-ZrB$_2$-fibre nozzle to evaluate its potential in rocket motors

Mater. Des., 109 (2016), pp. 709-717, 10.1016/j.jeurceramsoc.2016.04.039

Article   Download PDF   View Record in Scopus   Google Scholar

[13]   L.S. Walker, E.L. Corral

Self-generating high – temperature oxidation- resistant glass ceramic coatings for C-C composites using UHTCs

J. Am. Ceram. Soc., 97 (2014), pp. 3004-3011, 10.1111/jace.13017

CrossRef   View Record in Scopus   Google Scholar

[14]   D. Sciti, A.N. Murri, V. Medri, L. Zoli

Continuous C fibre composites with a porous ZrB$_2$ Matrix

Mater. Des., 85 (2015), pp. 127-134, 10.1016/j.matdes.2015.06.136

Article   Download PDF   View Record in Scopus   Google Scholar

[15]   L. Zoli, V. Medri, C. Melandri, D. Sciti

Continuous SiC fibers-ZrB$_2$ composites

J. Eur. Ceram. Soc., 35 (2015), pp. 4371-4376, 10.1016/j.jeurceramsoc.2015.08.008

Article   Download PDF   View Record in Scopus   Google Scholar

[16]   S.R. Levine, E.J. Opila, M.C. Halbig, J.D. Kiser, M. Singh, J.A. Salem

Evaluation of ultra-high temperature ceramics for aeropropulsion use

J. Eur. Ceram. Soc., 22 (2002), pp. 2757-2767, 10.1016/S0955-2219(02)00140-1

Article   Download PDF   View Record in Scopus   Google Scholar

[17]   Y. Ding, S. Dong, Q. Zhou, Z. Huang, D. Jiang

Preparation of C/SiC composites by hot pressing, using different C fiber content as reinforcement

J. Am. Ceram. Soc., 89 (2006), pp. 1447-1449, 10.1111/j.1551-2916.2005.00872.x

CrossRef   View Record in Scopus   Google Scholar

[18]   V. Medri, C. Capiani, D. Gardini

Slip casting of ZrB$_2$–SiC composite aqueous suspensions

Adv. Eng. Mater., 12 (2010), pp. 210-215, 10.1002/adem.200900275

CrossRef   View Record in Scopus   Google Scholar

[19]   D.G. Munz, J.L.J. Shannon, R.T. Bubsey

Fracture toughness calculations from maximum load in four point bend tests of chevron notch specimens

Int. J. Fract., 16 (1980), pp. R137-R141, 10.1007/bf00013393

CrossRef   View Record in Scopus   Google Scholar

[20]   W.G. Fahrenholtz, G.E. Hilmas, I.J. Talmy, J.A. Zaykoski

Refractory diborides of zirconium and hafnium

J. Am. Ceram. Soc., 90 (2007), pp. 1347-1364, 10.1111/j.1551-2916.2007.01583.x

CrossRef   View Record in Scopus   Google Scholar

[21]   L. Zoli, D. Sciti, L.-A. Liew, K. Terauds, S. Azarnoush, R. Raj

Additive manufacturing of ceramics enabled by flash pyrolysis of polymer precursors with nanoscale layers

J. Am. Ceram. Soc., 99 (2016), pp. 57-63, 10.1111/jace.13946

CrossRef   View Record in Scopus   Google Scholar

[22]   L. Silvestroni, D. Dalle Fabbriche, C. Melandri, D. Sciti

Relationships between carbon fiber type and interfacial domain in ZrB$_2$-based ceramics

J. Eur. Ceram. Soc., 36 (2016), pp. 17-24, 10.1016/j.jeurceramsoc.2015.09.026

Article   Download PDF   View Record in Scopus   Google Scholar

[23]   A. Rezaie, W.G. Fahrenholtz, G.E. Hilmas

The effect of graphite addition on oxidation of ZrB$_2$-SiC in air at 1500 °C

J. Eur. Ceram. Soc., 33 (2013), pp. 413-421, 10.1016/j.jeurceramsoc.2012.09.016

Article   Download PDF   View Record in Scopus   Google Scholar

[24]   X. Zhang, L. Xu, S. Du, W. Han, J. Han

Crack-healing behavior of zirconium diboride composite reinforced with silicon carbide whiskers

Scripta Mater., 59 (2008), pp. 1222-1225, 10.1016/j.scriptamat.2008.08.013

Article   Download PDF   View Record in Scopus   Google Scholar